Irina A. Anokhina, Irina E. Animitsa, Anastasia F. Buzina,
Vladimir I. Voronin,Vladimir B. Vykhodets, Tatyana E. Kurennykh, Yuri P. Zaikov
Chimica Techno Acta. 2020. Vol. 7, no. 2. P. 51–60.
ISSN 2409–5613

DOI: 10.15826/chimtech.2020.7.2.02

Irina A. Anokhina,[ab] Irina E. Animitsa,[ab*]
Anastasia F. Buzina,[a] Vladimir I. Voronin,[c]
Vladimir B. Vykhodets,[c] Tatyana E. Kurennykh,[c]
Yuri P. Zaikov[ab]

[a] Ural Federal University,
19 Mira St., Yekaterinburg, 620002, Russia
[b] Institute of High Temperature Electrochemistry
of the Ural Branch of the Russian Academy of Sciences,
20 Akademicheskaya St., Yekaterinburg, 620990, Russia
[c] Institute of Metal Physics
of the Ural Branch of the Russian Academy of Sciences,
18 S. Kovalevskoy St., Yekaterinburg, 620108, Russia
**e-mail: irina.animitsa@urfu.ru*

Synthesis, structure and electrical properties of Li^+-doped pyrochlore $Gd_2Zr_2O_7$

The pyrochlore $Gd_{1.55}Li_{0.45}Zr_2O_{6.55}$ was prepared by the solution and solid-state methods. The introduction of lithium in the Gd-sublattice led to decrease in the lattice parameter a = 10.4830(8) Å in comparison with $Gd_2Zr_2O_7$ (a =10.5346(2) Å). Monitoring of the lithium content in the sample during heat treatments showed a loss of lithium at temperatures above 1100 °C, so, to maintain the stoichiometry of lithium the low temperature sintering methods are required. The sample $Gd_{1.55}Li_{0.45}Zr_2O_{6.55}$ exhibited a predominant oxygen-ion transport over a wide range of temperatures. Although doping did not lead to an increase in the oxygen-ion conductivity compared to $Gd_2Zr_2O_7$, it caused the suppression of the hole conductivity.

Keywords: gadolinium zirconate $Gd_2Zr_2O_7$, pyrochlore, Li^+-doping, conductivity.

Received: 08.04.2020. Accepted: 20.05.2020. Published: 30.06.2020.

Introduction

The use of molten salt electrolytes opens up new ways of implementing resource-efficient waste disposal processes that are safe for humans and the environment, including those for recycling radioactive substances and organic compounds [1–3]. Electrochemical methods have a minimal environmental hazard and allow the creation of controlled, closed process circuits. For instance, the development of oxygen sensors is required for the measurement of oxygen concentration during chemical processes or direct measurement of the oxygen content in the process gas [4]. However, this problem has not been solved yet. Currently used materials for an oxygen ion activity sensor are susceptible to corrosion in halide-based melts, therefore they are ineffective because they cannot provide precise control of technological process

parameters [5, 6]. To implement modern, environmentally friendly technological developments, new materials that work under extreme conditions (high temperatures, aggressive environments) are needed.

From the point of view of the possible use of the material as an O^{2-} sensor for Li^{+}-halide melts, the $Gd_2Zr_2O_7$ crystalline matrix with a pyrochlore structure is of interest for investigation. Gadolinium zirconate $Gd_2Zr_2O_7$ has attracted considerable attention of scientists in the last few years because of its high thermochemical stability and structural flexibility [7, 8]. In this work, we studied the structure and electrical properties of the Li^{+}-doped compound $Gd_{1.55}Li_{0.45}Zr_2O_{6.55}$ in comparison with the undoped $Gd_2Zr_2O_7$. Lithium was chosen as a dopant for two reasons: to create the oxygen deficiency and to prevent the possibility of ion exchange in Li^{+}-containing melts.

Experimental

The phases $Gd_2Zr_2O_7$ and $Gd_{1.55}Li_{0.45}Zr_2O_{6.55}$ were obtained by the solid-state method and Li-doped sample was also obtained by the modified Pechini method using glycerol-nitrate technique. Starting reagents Gd_2O_3 (99.998%, VEKTON, Russia), ZrO_2 (99.99%, REACHIM, Russia) were preliminarily calcined at 600 °C for 3h, Li_2CO_3 (99.99%, VEKTON, Russia) at 400 °C for 2 h. The synthesis was carried out in the temperature range of 700–1300 °C with a step of 100 °C with intermediate grindings. The phase composition was monitored by the X-ray analysis after each stage.

The sample with nominal stoichiometry $Gd_{1.55}Li_{0.45}Zr_2O_{6.55}$ was synthesized by a citrate-nitrate technique based on the Pechini method. In addition, glycerol was used as a fuel and a ligand in complexation reactions. The preliminarily calcined gadolinium oxide, zirconium oxide and lithium carbonate were weighed according to the stoichiometry and then the powders were dissolved in an excess of concentrated nitric acid, moreover, microwave treatment was used to dissolve Gd_2O_3 and ZrO_2 upon heating at 80–100 °C. Then, the required amount of distilled water was added in order to reach the cations' concentration of ~1 mol/L. Then citric acid and glycerol were added. The solutions were mixed and heated at the temperature of 200 °C until spontaneous combustion occurred. To remove residual carbon, the powder were further annealed at the temperature of 700 °C. The final product was obtained by further heat treatments in the temperature range of 800–1300 °C with intermediate grinding in an agate mortar in ethanol.

X-ray analysis was carried out to control the phase composition and to determine the structural parameters of the studied samples. X-ray diffraction patterns were obtained at room temperature on a Rigaku MiniFlex600 diffractometer (Rigaku, Japan) with Cu Kα radiation in the range of 2θ = 10–80° with a step of 0.01° and at a scanning rate of 0.5 °/min. Calculation of interatomic distances and determination of unit cell parameters were performed using FullProf software.

The elemental analysis for the samples $Gd_2Zr_2O_7$ and $Gd_{1.55}Li_{0.45}Zr_2O_{6.55}$ was carried out by set of methods:

— Chemical analysis for gadolinium and zirconium was carried out after each annealing temperature by inductively coupled plasma atomic emission spectroscopy on an Optima 4300 DV Perkin Elmer spectrometer, USA. The 0.1 g sample was dissolved in a mixture of concentrated sulfuric

acid and ammonium sulfate in the ratio of 3:2 by weight.

— The concentration of lithium in the samples was measured by nuclear reaction analysis (NRA) technique using a 2 MV Van-de-Graff accelerator. The reaction ^{7}Li (p, α) ^{4}He was used. The particle energy in the primary beam of protons was 762 keV. An incident beam was 2 mm in diameter. For the experiments, the powders were pressed into indium plate. As a result, a layer at least 2 μm thick containing only oxide particles was formed near the outer surface of the sample. The flat surface of the samples was perpendicular to the axis of the primary beam. Products of nuclear reaction were registered by a silicon surface-barrier detector with the registration angle of 160°. The irradiation dose was determined using a secondary monitor with the statistic error of about 1% [9]. The lithium concentration was determined by comparing the spectra from the samples to be measured and the reference sample with a constant (in depth) impurity concentration. The sample Li_2ZrO_3 was used as the reference sample, in which the lithium content was taken equal to 33.33 at.%. The concentration of light elements was calculated using the stopping power data for the examined samples [10]. The techniques of measurement and calculation of light element concentrations were described in more details in [11].

Conductivity measurements were performed using cylindrical disc-shaped specimens with a diameter of 8–10 mm and a thickness of ~ 2 mm, which were pressed at 2.8 MPa and then calcined at temperature of 1500 °C for 5 hours ($Gd_2Zr_2O_7$) and at temperature of 1100 °C ($Gd_{1.55}Li_{0.45}Zr_2O_{6.55}$) for 5 hours in case of the microwave sintering. The density of ceramic samples was measured by hydrostatic weighing in kerosene. $Gd_2Zr_2O_7$ ceramics had a relative density of 93–96%, and the $Gd_{1.55}Li_{0.45}Zr_2O_{6.55}$ sample had a relative density of 70%.

Electrical conductivity of the studied samples was measured by the method of electrochemical impedance in a two-electrode cell using an Impendancemeter Z-500PX (Elins, Chernogolovka) over a frequency range of 100 Hz — 1 MHz at the temperature range of 300–1000 °C. The platinum paste was applied on both sides of the sintered pellets and calcined at 900 °C for 3 hours.

The resistance was found by extrapolating the impedance spectrum to the real axis using ZView2 software. The electrical conductivity was calculated by the well-known formula: $\sigma = l / (SR)$, where R is the resistance of the sample, l is its thickness, S is the cross-sectional area. Conductivity measurements were carried out in air and argon.

Results and discussion

Structural features and phase characterization

Pyrochlore phase $Gd_2Zr_2O_7$

The X-ray diffraction pattern of the $Gd_2Zr_2O_7$ sample obtained after heat treatment at 1500 °C is shown in Fig. 1.

The X-ray diffraction pattern contains intense reflections that correspond to the structure of fluorite, and a set of superstructural lines with low intensity, characterizing the structure of pyrochlore. The intensity of these reflections is determined by the difference in the scattering abilities of the A- and B-cations of the $A_2B_2O_7$ compound; in addition, their intensities are also determined by the dis-

placement of O1 atoms from the ideal position (3/8 1/8 1/8). The presence of superstructural reflections on the X-ray diffraction pattern confirms the formation of the pyrochlore structure. However, in the model of perfectly ordered pyrochlore, the treatment of X-ray diffraction patterns does not give good agreement with the experimental data. Therefore, the following assumptions were made:

1) The possibility of anti-structural defects in the cationic sublattice, i.e. part of the Gd atoms in A-sites replaces the same part of Zr atoms in B-sites and vice versa. In this case, the total number of cations in the lattice remains constant.

2) The existence of the defects in the oxygen sublattice; in addition, taking into account the results of investigations in [12], it was suggested that oxygen atoms could be redistributed between the O1 position and the O3 vacant position in the ideal lattice. The results of fitting are shown in Fig. 1, and the refined structural parameters are shown in Table 1. The crystal lattice is shown in Fig. 2.

It can be seen (Table 1), that 20% inversion of atoms at the A- and B-sublattices is observed, while 10% of oxygen atoms move from O1 sites to the initially vacant

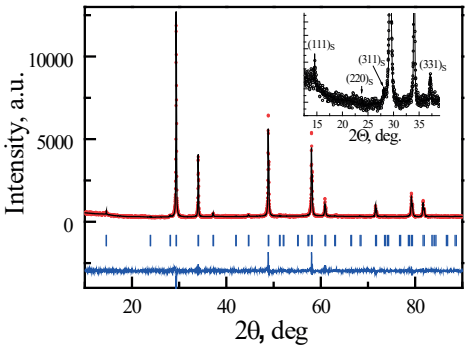

Fig. 1. Experimental (circles) and calculated (line) X-ray diffraction patterns of the $Gd_2Zr_2O_7$ sample at room temperature. The dashes are the angular positions of the reflections. The bottom line is the difference between the calculated and the experimental data. The inset shows a fragment of an X-ray image on an enlarged scale showing superstructural reflections

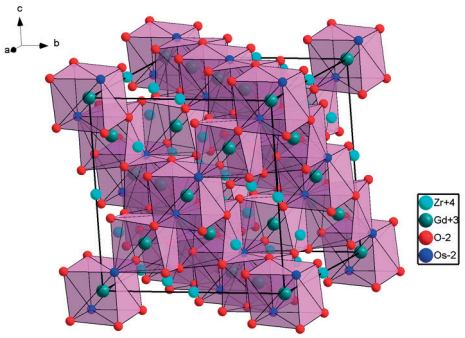

Fig. 2. The crystal structure of $Gd_2Zr_2O_7$

Table 1

The refined coordinates of atoms for $Gd_2Zr_2O_7$ in a cubic unit cell (space group: $Fd\bar{3}m$) with a cell parameter a = 10.5346(2) Å

Atom	Wyckoff symbol	*x*/*a*	*y*/*b*	*z*/*c*	Occupancy
Gd	16c	0.000	0.000	0.000	0.797(3)
Zr	16c	0.000	0.000	0.000	0.203(3)
Zr	16d	0.500	0.500	0.500	0.797(3)
Gd	16d	0.500	0.500	0.500	0.203(3)
O1	48f	0.400(1)	0.125	0.125	2.72(4)
O2	8a	0.125	0.125	0.125	0.500(0)
O3	8b	0.375	0.375	0.375	0.28(4)

R_p = 6.27 R_{wp} = 8.00 R_{exp} = 4.83 R_b = 5.57 R_f = 6.61 Chi^2 = 2.77

O3 sites. The results obtained are in good agreement with published data. For example, it was indicated [13] that the maximum degree of disordering of cationic positions in $Gd_2Zr_2O_7$ can reach 40%. Such structural features of $Gd_2Zr_2O_7$ are determined by the following conditions. The ordered structure of pyrochlore is formed only at $R_A / R_B \geq 1.46$ [13]. In the case of $Gd_2Zr_2O_7$, the ratio of the cation radii is $R_{Gd} / R_{Zr} = 1.46$ (the radius of Gd^{3+} in the 8-fold coordination is 1.053 Å, and the radius of Zr^{4+} in the 6-fold coordination is 0.72 Å [14]). Thus, according to geometric criteria, the $Gd_2Zr_2O_7$ phase is located near the boundary of the pyrochlore–fluorite transition, which leads to the inversion of atoms in the sublattices and 100% ordering is not observed. Moreover, the degree of disordering in the cationic and oxygen sublattices depends on the regimes of heat treatments [15–17]. High-temperature studies of the structure are necessary, and neutron diffraction experiments are needed to detect the changes in the oxygen sublattice.

The phase $Gd_{1.55}Li_{0.45}Zr_2O_{6.55}$

The evolution of XRD patterns for the sample $Gd_{1.55}Li_{0.45}Zr_2O_{6.55}$, prepared by solution and solid-state techniques, is shown in Fig. 3. As can be seen, the fluorite phase was obtained at 700 °C for the sample, prepared by solution method; the impurity phases Li_2ZrO_3 and $LiGdO_2$ were also found in traces amounts, which disappeared upon annealing at 900 °C. A single-phase sample with the pyrochlore structure was obtained at 1100 °C. At the same time, the formation of a fluorite phase for the sample, prepared by solid-state method, was observed at the temperature of 1100 °C; the gadolinium and zirconium oxides were present up to the temperature of 1200 °C. A single-phase sample was obtained only at 1300 °C. Thus, the solution method makes it possible to reduce the synthesis temperature of a single-phase sample by 200 °C.

Chemical composition of the obtained phases was monitored at all stages of the heat treatments. It was found that at all stages of the synthesis and sintering the atomic ratios of gadolinium and zirconium did not change and remained in exact accordance with the theoretical composition. However, the lithium content varied depending on the annealing temperature.

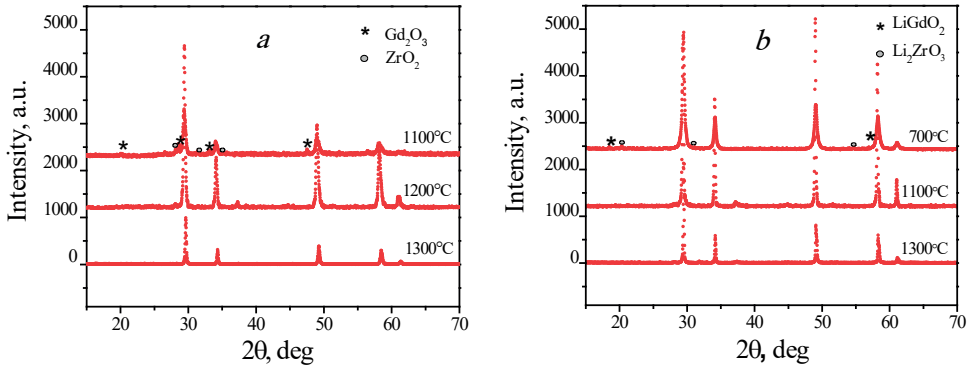

Fig. 3. The evolution of the X-ray diffraction patterns of the $Gd_{1.55}Li_{0.45}Zr_2O_{6.55}$ sample at different synthesis temperatures for *a*) the solid-state method, *b*) the modified Pechini method

Table 2 presents the data on the lithium content obtained by the method of nuclear reactions. As can be seen, lithium loss does not occur up to temperatures of 1100 °C, but at higher heat treatment temperatures, stoichiometry is shifted, and lithium is not detected in the samples at annealing temperatures of 1300 °C. These data made it possible to select the necessary temperature-time sequences for synthesis of Li^+-containing phase with a given lithium stoichiometry. Thus, for the solid-phase synthesis method, it is appropriate to calcine the powder at temperatures up to 1000–1100 °C, press it into a pellet and then prepare a single-phase sample by microwave sintering at 1000–1100 °C.

X-ray diffraction pattern refinement results of the sample $Gd_{1.55}Li_{0.45}Zr_2O_{6.55}$, obtained under microwave heat treatment at 1000 °C for 5 hours, are shown in Fig. 4.

The sample has a pyrochlore structure, but the superstructural lines (111, 311, 331, 511, 531, 444) are very weak, which indicates a disordering of the pyrochlore structure. The lattice parameter was smaller compared to the undoped phase $Gd_2Zr_2O_7$.

Electrical measurements

Fig. 5 shows the evolution of the impedance spectra of $Gd_{1.55}Li_{0.45}Zr_2O_{6.55}$ for various temperature ranges. As can be seen, in the general case, several relaxation processes can be distinguished, and the shape of the impedance diagram changed with temperature. At high temperatures (T > 800 °C), a semicircle, which does not start from zero and can be attributed to the grain boundary response, is well distinguished, the capacitance for this process corresponds to a value of ~10^{-8} F/cm. With decreasing temperature, the low frequency arc was not clearly visible, and the first semicircle, starting from zero, become more pronounced. This first semicircle can

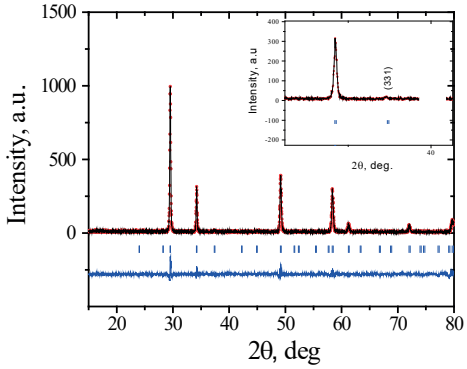

Fig. 4. Experimental (circles) and calculated (solid line) X-ray diffraction patterns of the $Gd_{1.55}Li_{0.45}Zr_2O_{6.55}$ sample at room temperature. The dashes are the angular positions of the reflections. The bottom line is the difference between the calculation and the experimental data. The inset shows a fragment of an X-ray image on an enlarged scale with superstructural reflections

Table 2

The lithium content (wt.%) according to the method of nuclear microanalysis for the sample with the composition of $Gd_{1.55}Li_{0.45}Zr_2O_{6.55}$, obtained by various heat treatments

The concentration of lithium (wt.%)			
Theoretical value	Experimental value		
	900 °C	1100 °C	1300 °C
0.587	0.65 ± 0.05	0.52 ± 0.04	0

be attributed to the relaxation process due to the grain volume resistance with capacity of ~ 10^{-11} F/cm.

Thus, the impedance of the studied electrochemical cell consists of the grain volume resistance R_g with a constant phase element CPE_g parallel to it, the resistance of the grain boundaries R_{gb} with the parallel constant phase element CPE_{gb} and the electrode impedance Z_{el} (the equivalent circuit is shown in Fig. 5).

Doping with lithium did not affect the general shape of the impedance spectra

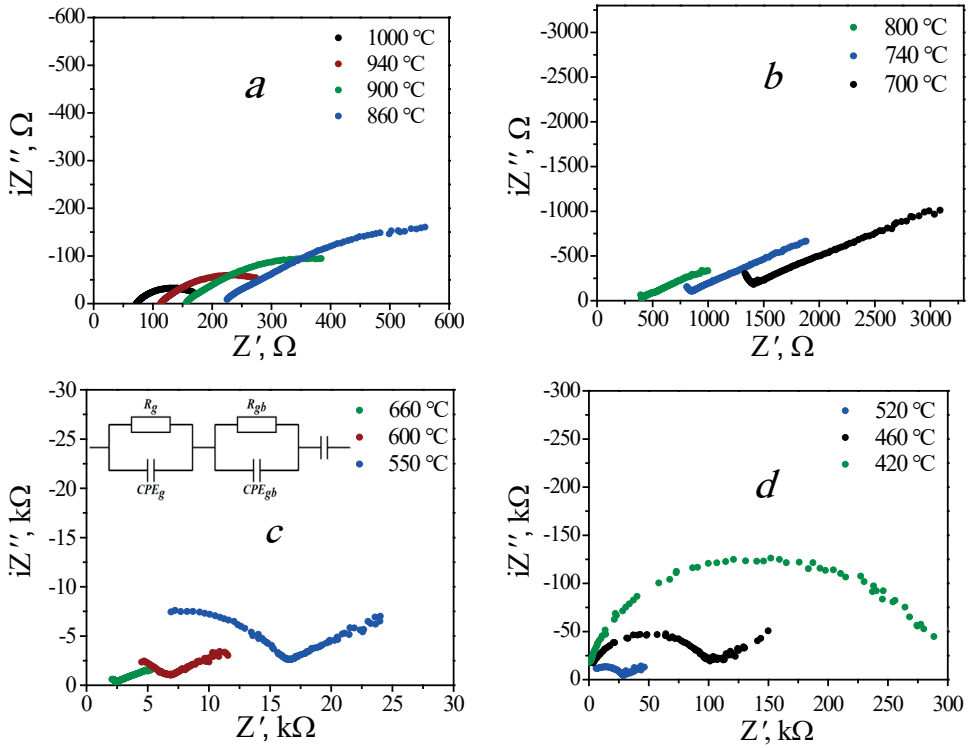

Fig. 5. Impedance spectra for $Gd_{1.55}Li_{0.45}Zr_2O_{6.55}$ at (*a*) 860–1000 °C, (*b*) 700–800 °C, (*c*) 560–660 °C, (*d*) 400–520 °C in air

in comparison with the undoped sample. However, it should be noted, that the impedance spectra of the Li^+-containing sample, obtained by the solution method, was significantly different. The large semicircle was observed due to the resistance of the grain boundaries over the main region of the studied frequencies (Fig. 6). Therefore, the grain volume resistance could not be determined.

Since the ceramics of the studied phases $Gd_2Zr_2O_7$ and $Gd_{1.55}Li_{0.45}Zr_2O_{6.55}$ had different porosities, it was necessary to normalize the values for the less dense $Gd_{1.55}Li_{0.45}Zr_2O_{6.55}$ sample to 95–100% density. Conductivity was recalculated according to the known relation: $\sigma_{measured}=\sigma_o \cdot d^2$, where d is relative density, $\sigma_{measured}$ is the apparent conductivity of the porous material, σ_o is the intrinsic conductivity of the dense

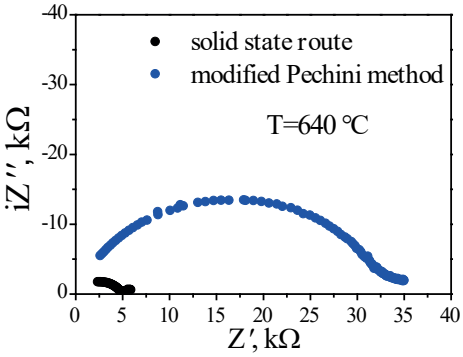

Fig. 6. The impedance plot of $Gd_{1.55}Li_{0.45}Zr_2O_{6.55}$ at 640°C. The samples were synthesized by solid state route and modified Pechini method

material [18]. A comparison of the temperature dependences of the bulk conductivities of the $Gd_{1.55}Li_{0.45}Zr_2O_{6.55}$ sample obtained by solid-state synthesis and the undoped $Gd_2Zr_2O_7$ is shown in Fig. 7.

It can be seen, that the introduction of dopant does not lead to an increase in the total electrical conductivity in comparison with undoped $Gd_2Zr_2O_7$.

In order to clarify the nature of the dominant type of charge carrier, the measurements of electrical conductivity were performed in argon (pO_2 = 10^{-5} atm). As can be seen (Fig. 7), the electrical conductivity of the undoped sample of $Gd_2Zr_2O_7$ in argon was lower than in air. This suggests that in air the $Gd_2Zr_2O_7$ sample is characterized by mixed ion-hole type conductivity. The obtained results are in good agreement with the literature data [19], where it was shown that the conductivity in air is mixed with the ionic transport number t_{ion} = 0.57 at 780 °C, and the contribution of electronic conductivity increases at high temperatures. Assuming that the conductivity in argon atmosphere at low temperatures is predominantly ionic, the estimation of the ion transport number in air gives the value t_{ion} = 0.98 at 500 °C, which correlates well with literature data [20].

On the contrary, for Li^+-doped sample, the conductivities measured in argon and in air are almost equal. This indicates predominantly ionic conductivity. However, comparing the ionic conductivities, measured in argon, it can be seen that the ionic conductivity of the Li-doped sample is lower than that of gadolinium zirconate $Gd_2Zr_2O_7$. This indicates lower mobility of oxygen vacancies in the $Gd_{1.55}Li_{0.45}Zr_2O_{6.55}$ sample. The decrease in mobility is probably due to the interaction of oxygen vacancies $V_O^{\bullet\bullet}$ with the acceptor defect Li''_{Gd}, which has the opposite charge. In this case, the formation of a neutral associate $\{Li''_{Gd} \cdot V_O^{\bullet\bullet}\}^{\times}$ occurs. So, trapping leads to a decrease in the mobility of oxygen vacancies and, accordingly, to a decrease in the conductivity.

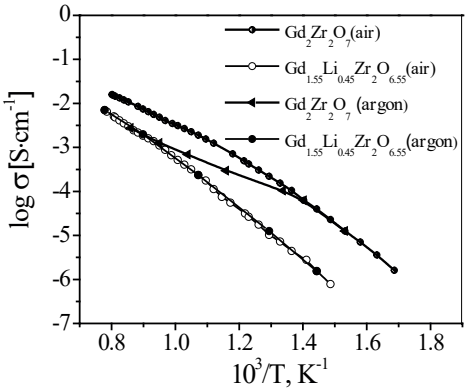

Fig. 7. Temperature dependencies of conductivities for $Gd_2Zr_2O_7$ and $Gd_{1.55}Li_{0.45}Zr_2O_{6.55}$

Conclusions

The phase with the pyrochlore structure $Gd_{1.55}Li_{0.45}Zr_2O_{6.55}$ was obtained. Monitoring of lithium content in the sample by the nuclear reaction method allowed the development of synthesis methods with a given lithium stoichiometry. The introduction of lithium into the Gd-sublattice led to a decrease in the lattice parameter a = 10.4830 (8) Å in comparison with $Gd_2Zr_2O_7$ (a = 10.5346(2) Å). The Li^+-doped sample was characterized by predominant oxygen-ion transport over a wide range of temperatures. Although doping did not increase the oxygen-ion conductivity, it suppressed hole conductivity.

Acknowledgements

The reported study was funded by RFBR and Sverdlovsk region, project number 20-43-660033a.

References

1. Merwin A, Williamson MA, Willit JL, Chidambaram D. Review-Metallic lithium and the reduction of actinide oxides. Journal of the Electrochemical Society. 2017;164(8):H5236–46.
   DOI: 10.1149/2.0251708jes
2. Choi EY, Lee J. Complete reduction of high-density UO_2 to metallic U in molten Li_2O-LiCl. Journal of Nuclear Materials. 2017;494:439–47.
   DOI: 10.1016/j.jnucmat.2017.07.036
3. Willit JL, Miller WE, Battles JE. Electrorefining of uranium and plutonium — A literature review. Journal of Nuclear Materials. 1992;195(3):229–49.
   DOI: 10.1016/0022–3115(92)90515-M
4. Choi EY, Choi IK, Hur JM, Kang DS, Shin HS, Jeong SM. In situ electrochemical measurement of O^{2-} concentration in molten Li_2O/LiCl during uranium oxide reduction process. Electrochemical and Solid-State Letters. 2012;15(3):E11 — E13.
   DOI: 10.1149/2.016203esl
5. Cho SH, Kim DY, Kwon S, Yoon BH, Lee JH. High-temperature corrosion characteristics of yttria-stabilized zirconia material in molten salts of LiCl-Li_2O and LiCl-Li_2O-Li. Journal of Nuclear Science and Technology. 2018;55(1):97–103.
   DOI: 10.1080/00223131.2017.1383214
6. Cho SH, Kim SW, Kim DY, Lee JH, Hur JM. Hot corrosion behavior of magnesia-stabilized ceramic material in a lithium molten salt. Journal of Nuclear Materials. 2017;490:85–93.
   DOI: 10.1016/j.jnucmat.2017.04.012
7. Lehmann H, Pitzer D, Pracht G, Vassen R, Stoever D. Thermal conductivity and thermal expansion coefficients of the lanthanum rare-earth-element zirconate system. Journal of the American Ceramic Society. 2003;86(8):1338–44.
   DOI: 10.1111/j.1151–2916.2003.tb03473.x
8. Radha AV, Ushakov SV, Navrotsky A. Thermochemistry of lanthanum zirconate pyrochlore. Journal of Materials Research. 2009;24(11):3350–7.
   DOI: 10.1557/jmr.2009.0401
9. Volkov VN, Vykhodets VB, Golubkov IK, Klotsman SM, Lerkh PV, Pavlov VA. Accurate light ion beam monitoring by backscattering. Nucl Instrum and Meth. 1983;205:73–7.
   DOI: 10.1016/0167–5087(83)90175–8
10. Ziegler JF. Biersack JP. The stopping and ranges of ions in matter. New York: Pergamon Press; 1977.
11. Vykhodets VB, Klotsman SM, Levin AD. Oxygen diffusion in α-Ti: II. The calculation of the concentration profile of impurities in the nuclear microanalysis. The Phys. Metal & Metallogr. 1987;64:920–4.
12. Wuensch BJ, Eberman KW, Heremans C, Ku EM, Onnerud P, Yeo EME, Haile SM, Stalick JK, Jorgensen JD. Connection between oxygen-ion conductivity of pyrochlore fuel-cell materials and structural change with composition and temperature. Solid State Ionics. 2000;129:111–33.
   DOI: 10.1016/S0167-2738(99)00320–3

13. Zhang FX, Lang M, and Ewing RC. Atomic disorder in $Gd_2Zr_2O_7$ pyrochlore. Applied Physics Letters. 2015;106:191902.
DOI: 10.1063/1.4921268
14. Shannon RD. Revised effective ionic radii and systematic studies of interatomic distances in halides and chalcogenides. Acta Cryst. 1976;A32:751–67.
DOI: 10.1107/S0567739476001551
15. Michel D, Perez M, Jorba, Collongues R. Etude de la Transformation Ordre — De´sordre de la Structure Fluorite a` la Structure Pyrochlore pour des Phases (1-*x*) $ZrO_{2-x}Ln_2O_3$. Mater Res Bull. 1974;9:1457–68.
16. Uehara T, Koto K, Emura S, Kanamaru F. EXAFS study of fluorite and pyrochlore compounds in the system ZrO — GdO. Solid State Ionics. 1987;23:331–7.
DOI: 10.1016/0167–2738(87)90012–9
17. Scheetz BE, White WB. Characterization of anion disorder in zirconate $A_2B_2O_7$ compounds by Raman spectroscopy. J. Am. Ceram. Soc. 1979;62:468–70.
DOI: 10.1111/j.1151–2916.1979.tb19107.x
18. Khal HEl, Cordier A, Batis N, Siebert E, Georges S, Steil MC. Effect of porosity on the electrical conductivity of LAMOX materials. Solid State Ionics. 2017;304:75–84.
DOI: 10.1016/j.ssi.2017.03.028
19. Catlow CRA. Defects and disorder in crystalline and amorphous solids. Springer Science+Business Media Oordrecht; 1994.
DOI: 10.1007/978-94-011-1942-9
20. Van Dijk MP, De Vries KJ, Burggraaf AJ. Electrical conductivity and defect chemistry of the system $(Tb_xGd_{1-x})_2Zr_2O_{7+y}$ ($O \leqq x \leqq 1; O \leqq y < 0.25$). Solid State Ionics. 1985;16:211–4.
DOI: 10.1016/0167–2738(85)90045–1